Available online at www.sciencedirect.com
SCIENCE DIRECT®
Journal of Sound and Vibration 290 (2006) 572–596
JOURNAL OF SOUND AND VIBRATION
www.elsevier.com/locate/jsvi

A hydroelasticity method for vibrating structures containing and/or submerged in flowing fluid

B. Uğurlu, A. Ergin*

Faculty of Naval Architecture and Ocean Engineering, Istanbul Technical University, Maslak, 34469 Istanbul, Turkey

Received 11 March 2004; received in revised form 30 March 2005; accepted 5 April 2005
Available online 24 August 2005

Abstract

This paper presents a method for investigating the dynamics of elastic structures containing and/or submerged in flowing fluid. The method presented is based on a boundary integral equation method in conjunction with the method of images, in order to impose appropriate boundary condition on the fluid's free surface. The method of analysis can be applied to any shape of cylindrical structure partially in contact with flowing fluid. In the analysis of the linear fluid–structure system, it is assumed that the fluid is ideal, i.e., inviscid, incompressible and its motion is irrotational. It is assumed that the flexible structure vibrates in its in vacuo eigenmodes when it is in contact with flowing fluid, and that each mode gives rise to a corresponding surface pressure distribution on the wetted surface of the structure. The in vacuo dynamic properties of the *dry* structure are obtained by using a standard finite element software. In the *wet* part of the analysis, the wetted surface is idealized by using appropriate boundary elements, referred to as hydrodynamic panels. The fluid–structure interaction effects are calculated in terms of the generalized added mass coefficients, generalized Coriolis fluid force coefficients and generalized centrifugal fluid force coefficients. In order to demonstrate the applicability of the proposed method, a circular cylindrical shell, simply supported at both ends, was adopted for the calculations. The cylindrical shell was considered separately with rigid and flexible extensions at its ends. To assess the influence of flowing fluid on the dynamic behavior of the shell structure, the non-dimensional eigenfrequencies and associated eigenmodes are presented as a function of the non-dimensional fluid velocity. The predictions compare well with available analytical calculations found in the literature.

*Corresponding author. Fax: +90 212 285 6454.
E-mail address: ergina@itu.edu.tr (A. Ergin).

0022-460X/$ - see front matter © 2005 Elsevier Ltd. All rights reserved.
doi:10.1016/j.jsv.2005.04.028

1. Introduction

Dynamic behavior of structures partially or completely in contact with flowing fluid is of great importance in a variety of engineering applications, such as, vibration of flexible pipelines conveying fluid, heat exchanger tubes in axial flow and containing flowing fluid, inflatable dams in the presence of flowing water, etc. All these vibration problems are complicated by the interactions that take place between structure and fluid. This is due to the vibration of the structural surface in contact with the fluid medium imparting motion to the fluid, thus altering its pressure, and, hence, inducing reactive forces on its surface.

It is of practical importance to estimate the effect of the induced fluid loading on the dynamic state of the vibrating structure. When a body oscillates in an unbounded (and/or completely filled with) inviscid quiescent fluid, the hydrodynamic inertia forces are constants, independent of the frequency of vibration. However, in the case when the body oscillates in or near a free surface (and/or partially filled), the hydrodynamic inertia forces exhibit frequency dependence in the low-frequency region, but show a tendency towards a constant value in the high-frequency region. Furthermore, additional fluid–structure interaction forces occur when the fluid is flowing.

The response of shell structures immersed in or conveying flowing fluid has been extensively studied, and general reviews of the literature have been given by Païdoussis [1] and Païdoussis and Li [2]. Recent books by Païdoussis [3,4] provide a comprehensive treatment of the subject as well as a complete bibliography of all important work in the field.

Moreover, Amabili and Garziera [5] presented a study on the linear dynamic analysis of cylindrical shells with flowing fluid. They investigated the influence of various complicating effects, such as non-uniform edge boundaries; internal, external and annular flows; intermediate constraints, etc., on the dynamic response behavior of the structure. On the other hand, a three-part study, investigating the dynamics of cantilever cylinders in axial flow, has been reported. In the first part, Païdoussis et al. [6] presented some old and new experimental results, and a comparison with linear theory was made. In the second part [7], a weakly nonlinear equation of motion was derived. The fluid dynamic forces were introduced in terms of virtual work expressions, separately for the inviscid forces, and for the hydrostatic and frictional forces. The results of calculations based on this theoretical model were presented in Part 3 [8], by means of bifurcation diagrams, phase-plane plots and Poincaré maps. Amabili et al. [9] developed a geometrically nonlinear shell model to study stability of shells-containing incompressible flow. However, the fluid–structure interaction forces were calculated by using a linear potential theory. This study has been extended by Amabili et al. [10], for investigating the nonlinear stability of supported, circular cylindrical shells in a compressible, inviscid, subsonic flow. In an investigation by Amabili et al. [11], the nonlinear dynamics and stability of simply supported, circular cylindrical shells containing inviscid, incompressible fluid flow were studied. The linear potential flow theory was again applied to describe the fluid–structure interaction forces. Lakis and Selmane [12] presents a hybrid finite element method to investigate the large amplitude vibrations of orthotropic cylindrical shells subjected to flowing fluid. In this study, only the linear effects of the fluid were taken into account. Toorani and Lakis [13,14] presented a method, based on the finite element method, refined shell theories and linear fluid dynamic theory, to analyze the vibration of anisotropic laminated composite cylindrical shells subjected to internal and external incompressible, inviscid flowing fluid. Recently, Toorani and Lakis [15] used the same method and

presented the flow-induced vibration characteristics of the anisotropic laminated cylindrical shells partially or completely filled with a quiescent liquid or subjected to a flowing fluid.

This paper presents a method for investigating the dynamics of elastic structures containing and/or submerged in flowing fluid. The method presented is based on a boundary integral equation method together with the method of images in order to impose appropriate boundary condition on the fluid's free surface. The method proposed in this study is already successfully applied to structures partially filled with or partially submerged in a quiescent fluid (see Refs. [16–18]). In this study, therefore, the mathematical model is extended for taking into account the effect of axial fluid velocity. Furthermore, it should also be noted that the method proposed here can be applied to any shape of cylindrical structure partially in contact with internal and/or external flowing fluid, in contrast to the studies found in the literature.

In order to demonstrate the applicability of the proposed method, a circular cylindrical shell, simply supported at both ends, was adopted for the calculations. The cylindrical shell was considered, separately, with rigid and flexible extensions at its ends. A cylindrical shell with rigid extensions corresponds to a finite length, flexible cylindrical shell connected to infinitely long rigid cylindrical baffles, of the same diameter as the shell, at both ends. However, the cylindrical shell with flexible extensions coincides with one that is infinitely long and periodically supported. For the shell with flexible extensions, only the vibrational modes that are anti-symmetric with respect to each support are considered. Therefore, these modes have the same in vacuo frequencies as those of a simply supported, single-span cylindrical shell, and they are, also, the vibration modes with the lowest frequencies.

In this investigation, it is assumed that the fluid is ideal, i.e., inviscid, incompressible and its motion is irrotational. It is assumed that the flexible shell structure vibrates in its in vacuo eigenmodes when it is in contact with flowing fluid, and that each mode gives rise to a corresponding surface pressure distribution on the wetted surface of the structure. The in vacuo dynamic analysis entails the vibration of the shell in the absence of any external force and structural damping and the corresponding dynamic characteristics (e.g., natural frequencies and mode shapes) of the shell structure were obtained by using a standard finite element software (i.e., [19]).

At the fluid–structure interface, continuity considerations require that the normal velocity of the fluid is equal to that of the structure. The normal velocities on the wetted surface are expressed in terms of modal structural displacements and their derivatives, with respect to the x-coordinate (see Fig. 1), obtained from the in vacuo dynamic analysis. By using a boundary integral equation method the fluid pressure is eliminated from the problem, and the fluid–structure interaction forces are calculated in terms of the generalized hydrodynamic added mass coefficients (due to the inertia effect of fluid), generalized fluid damping coefficients (due to the Coriolis acceleration of fluid) and generalized fluid stiffness coefficients (due to the centrifugal effect of fluid). However, when the structure is in contact with an ideal, quiescent fluid, the fluid–structure interaction forces are only associated with the inertial effect of fluid, i.e., the fluid pressure on the wetted surface of the structure is in phase with the structural acceleration.

During this analysis, the wetted surface is idealized by using appropriate boundary elements, referred to as hydrodynamic panels. The generalized structural mass matrix is merged with the generalized hydrodynamic mass matrix, and the generalized structural stiffness matrix with the generalized fluid stiffness matrix. Then, the total generalized mass and stiffness matrices are used

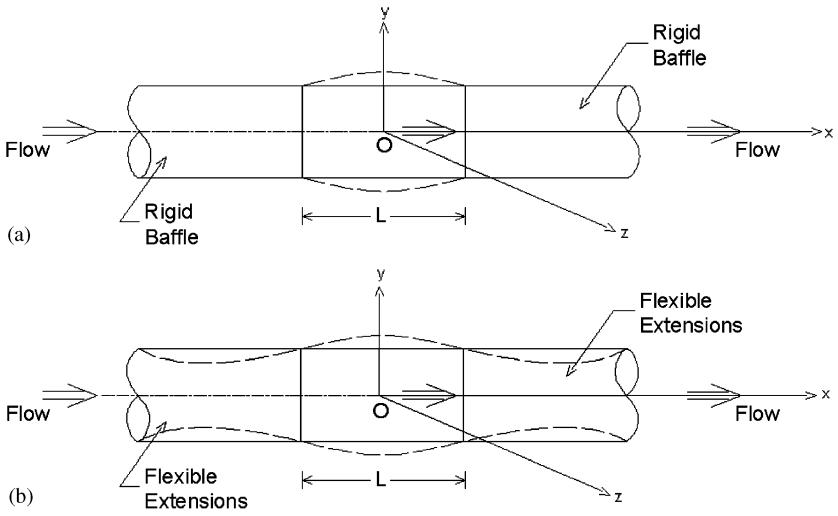

Fig. 1. Cylindrical shell conveying flowing fluid, (a) with rigid extensions and (b) with flexible extensions.

together with the generalized fluid damping matrix in solving the eigenvalue problem (Eq. (34)), for the elastic shell immersed in and/or containing flowing fluid. To assess the influence of flowing fluid on the dynamic behavior of the shell structure, the non-dimensional eigenfrequencies are presented as a function of the non-dimensional flow velocity. The associated eigenmodes are also presented for two different non-dimensional flow velocities. A very good comparison was obtained between the calculations of the present study and results found in the literature.

2. Mathematical model

2.1. Generalized equation of motion

The equation of motion describing the response of a discretized (finite element) structure to external excitation may be written as [20]

$$\mathbf{M}\ddot{\mathbf{U}} + \mathbf{C}_V\dot{\mathbf{U}} + \mathbf{K}\mathbf{U} = \mathbf{P}, \tag{1}$$

where $\mathbf{M}$, $\mathbf{C}_V$, $\mathbf{K}$ denote the mass, structural damping and stiffness matrices, respectively. The vectors $\mathbf{U}$, $\dot{\mathbf{U}}$ and $\ddot{\mathbf{U}}$ represent the structural displacements, velocities and accelerations, respectively, and the column vector $\mathbf{P}$ denotes the external forces. For the finite element structure, the displacements can be expressed as

$$\mathbf{U}^{\mathrm{T}} = [\mathbf{U}_1\ \mathbf{U}_2 \ldots \mathbf{U}_j \ldots \mathbf{U}_n], \tag{2}$$

where $\mathbf{U}_j$ represents the nodal displacements at the jth node, and n denotes the number of nodes used in the discretization. In a global xyz-coordinate system, for a shell element, each node can have 6dof: three translations u_x, u_y and u_z, and three rotations θ_x, θ_y and θ_z. Therefore, the nodal

displacements at the jth node may be written in the following form:

$$\mathbf{U}_j^{\mathrm{T}} = [u_x\ u_y\ u_z\ \theta_x\ \theta_y\ \theta_z]. \tag{3}$$

In an in vacuo analysis, the structure is assumed to vibrate in the absence of any structural damping and external forces reducing Eq. (1) to the form

$$\mathbf{M}\ddot{\mathbf{U}} + \mathbf{K}\mathbf{U} = \mathbf{0}. \tag{4}$$

The trial solution is expressed in the form of $\mathbf{U} = \mathbf{d}e^{i\omega t}$, and substituted in Eq. (4). By canceling the common factor $e^{i\omega t}$, one obtains the equation

$$(-\omega^2\mathbf{M} + \mathbf{K})\mathbf{d} = \mathbf{0}. \tag{5}$$

This equation describes the simple harmonic oscillations of the free undamped structure, and the in vacuo normal modes, $\mathbf{d}$, and natural frequencies, ω, are obtained from this equation.

The distortions of the structure may be expressed as the sum of the deflections in the normal modes,

$$\mathbf{U} = \mathbf{D}\mathbf{p}(t), \tag{6}$$

where $\mathbf{D}$ is the modal matrix whose columns are the in vacuo, undamped mode vectors, $\mathbf{d}$, of the structure. $\mathbf{p}$ is the principal coordinates vector. By substituting Eq. (6) into Eq. (1) and pre-multiplying by $\mathbf{D}^{\mathrm{T}}$, the following generalized equation in terms of the principal coordinates of the structure is obtained:

$$\mathbf{a}\ddot{\mathbf{p}}(t) + \mathbf{b}\dot{\mathbf{p}}(t) + \mathbf{c}\mathbf{p}(t) = \mathbf{Q}(t). \tag{7}$$

Here $\mathbf{a}$, $\mathbf{b}$, $\mathbf{c}$ denote the generalized mass, damping and stiffness matrices, respectively, and are defined as follows:

$$\mathbf{a} = \mathbf{D}^{\mathrm{T}}\mathbf{M}\mathbf{D}, \quad \mathbf{b} = \mathbf{D}^{\mathrm{T}}\mathbf{C}_V\mathbf{D}, \quad \mathbf{c} = \mathbf{D}^{\mathrm{T}}\mathbf{K}\mathbf{D}, \quad \mathbf{Q} = \mathbf{D}^{\mathrm{T}}\mathbf{P}. \tag{8}$$

It should be noted that the generalized mass, $\mathbf{a}$, and stiffness, $\mathbf{c}$, matrices are diagonal, but the generalized damping matrix, $\mathbf{b}$, is not necessarily diagonal. The generalized force matrix, $\mathbf{Q}(t)$ represents the fluid–structure interaction and all other external forces (e.g., wave forces, etc.), and it may be expressed as follows [21]:

$$\mathbf{Q}(t) = -(\mathbf{A}\ddot{\mathbf{p}}(t) + \mathbf{B}\dot{\mathbf{p}}(t) + \mathbf{C}\mathbf{p}(t)) + \Xi(t), \tag{9}$$

where $\mathbf{A}$, $\mathbf{B}$ and $\mathbf{C}$ are the generalized added mass, generalized fluid damping, and generalized fluid stiffness matrices, respectively, and $\Xi(t)$ denotes the generalized external force vector caused by waves, mechanical excitation, etc.

Thus, Eq. (7) may be rewritten in the form (see, for instance, Ref. [21])

$$(\mathbf{a} + \mathbf{A})\ddot{\mathbf{p}}(t) + (\mathbf{b} + \mathbf{B})\dot{\mathbf{p}}(t) + (\mathbf{c} + \mathbf{C})\mathbf{p}(t) = \Xi(t). \tag{10}$$

2.2. Formulation of the fluid problem

A right-handed Cartesian coordinate system, xyz, is adopted in the present study and it is shown in Fig. 1 for the circular cylindrical shell subjected to axial flow. The coordinate system is

fixed in space with its origin at O, and the x-axis coincides with the center line of the cylindrical shell in the longitudinal direction.

In the mathematical model, the fluid is assumed ideal, i.e., inviscid and incompressible, and its motion is irrotational and there exists a fluid velocity vector, $\mathbf{v}$, which can be defined as the gradient of the velocity potential function Φ as

$$\mathbf{v}(x,\ y,\ z,\ t) = \nabla\Phi(x,\ y,\ z,\ t). \tag{11}$$

The velocity potential Φ may be written as

$$\Phi = Ux + \phi. \tag{12}$$

Here the steady velocity potential Ux represents the effect of the mean flow associated with the undisturbed flow velocity U in the axial direction. Further, ϕ is the unsteady velocity potential associated with the perturbations to the flow field due to the motion of the flexible body, and satisfies the Laplace equation

$$\nabla^2\phi = 0, \tag{13}$$

throughout the fluid domain.

For the structure containing and/or submerged in flowing fluid, the vibratory response of the structure may be expressed in terms of principal coordinates as

$$\mathbf{p}(t) = \mathbf{p_0}e^{\lambda t}, \tag{14}$$

where $\mathbf{p_0}$ and λ are complex non-zero constants, and t is the time. The imaginary part of λ is the circular frequency of oscillations and its real part gives an exponential growth or decay. The velocity potential function due to the distortion of the structure in the rth in vacuo vibrational mode may be written as follows

$$\phi_r(x,\ y,\ z,\ t) = \phi_r(x,\ y,\ z)p_{0r}e^{\lambda t}, \quad r = 1, 2, \ldots, M, \tag{15}$$

where M represents the number of modes of interest, and p_{0r} is an unknown complex amplitude for the rth principal coordinate.

On the wetted surface of the vibrating structure the fluid normal velocity must be equal to the normal velocity on the structure and this condition for the rth modal vibration of the elastic structure containing or/and submerged in flowing fluid can be expressed as (see, for instance, Ref. [5])

$$\frac{\partial\phi_r}{\partial\mathbf{n}} = \left(\frac{\partial\mathbf{u}_r}{\partial t} + U\frac{\partial\mathbf{u}_r}{\partial x}\right)\cdot\mathbf{n}, \tag{16}$$

where $\mathbf{n}$ is the unit normal vector on the wetted surface and points into the region of interest. The vector $\mathbf{u}_r$ denotes the displacement response of the structure in the rth principal coordinate and it may be written as

$$\mathbf{u}_r(x,\ y,\ z,\ t) = \mathbf{u}_r(x,\ y,\ z)p_{0r}e^{\lambda t}, \tag{17}$$

where $\mathbf{u}_r(x, y, z)$ is the rth modal displacement vector of the median surface of the elastic structure, and it is obtained from the in vacuo analysis.

Substituting Eqs. (15) and (17) into Eq. (16), the following expression is obtained for the boundary condition on the fluid–structure interface

$$\frac{\partial \phi_r}{\partial \mathbf{n}} = \lambda \mathbf{u}_r(x, y, z) \cdot \mathbf{n} + U \frac{\partial \mathbf{u}_r(x, y, z)}{\partial x} \cdot \mathbf{n}. \tag{18}$$

In this study, it is assumed that the elastic structure vibrates at relatively high frequencies so that the effect of surface waves can be neglected. Therefore, the free surface condition (infinite frequency limit condition) for the perturbation potential can be approximated by

$$\phi_r = 0, \quad \text{on the free surface.} \tag{19}$$

The method of images [16,22] may be used, as shown in Fig. 2, to satisfy this boundary condition. By adding an imaginary boundary region, the condition given by Eq. (19) at the horizontal surface can be omitted; thus the problem is reduced to a classical Neumann case. It should be noted that, for the completely filled elastic structure, the normal fluid velocity cannot be arbitrarily specified. It has to satisfy the incompressibility condition

$$\iint_{S_W + S_{\text{im}}} \frac{\partial \phi_r}{\partial \mathbf{n}} \, \mathrm{d}S = 0, \tag{20}$$

where S_W and S_{im} represent the wetted and image surfaces of the elastic structure, respectively.

2.3. Evaluation of perturbation potential ϕ

The perturbation potential, ϕ, in a three-dimensional inviscid flow field due to the oscillating elastic structure can be expressed by means of a distribution of unknown constant source strength,

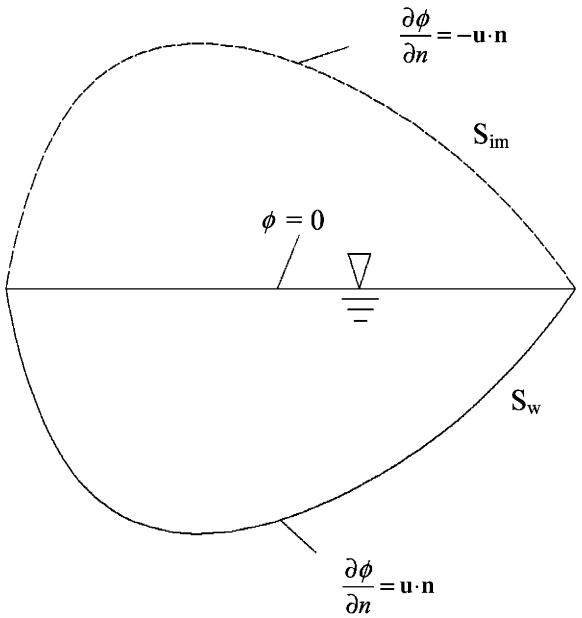

Fig. 2. Wetted surface and image boundary for a partially filled structure.

σ, over the wetted and image surfaces of the elastic structure (see, for example, Refs. [23,24]) in the following form:

$$\phi(\mathbf{r}) = \iint\limits_{S_W+S_{\text{im}}} \frac{\sigma(\mathbf{r}_0)}{R(\mathbf{r},\,\mathbf{r}_0)}\,\mathrm{d}S, \tag{21}$$

where

$$R = \left[(x-x_0)^2 + (y-y_0)^2 + (z-z_0)^2\right]^{1/2}$$

and $\mathbf{r} = (x, y, z)$ denotes the position vector of the field point within the fluid, $\mathbf{r}_0 = (x_0, y_0, z_0)$ is the position vector of a source point on the wetted/image surface of the structure.

The fluid–structure interaction problem may be separated into two parts: (i) the vibration of the elastic structure in a quiescent fluid, and (ii) the disturbance in the main axial flow due to the oscillation of the elastic structure. Thus, defining $\phi = \lambda\phi_1 + U\phi_2$, Eq. (18) may be divided into two parts as

$$\frac{\partial\phi_1}{\partial\mathbf{n}} = \mathbf{u}(x, y, z)\cdot\mathbf{n}, \tag{22}$$

$$\frac{\partial\phi_2}{\partial\mathbf{n}} = \frac{\partial\mathbf{u}(x, y, z)}{\partial x}\cdot\mathbf{n}, \tag{23}$$

where ϕ_1 denotes the displacement potential due to the vibration of the structure in a quiescent fluid, and ϕ_2 represents the disturbing effect of the term $\partial u/\partial x$ to the main axial flow field.

Substituting boundary conditions (22) and (23) into Eq. (21), the unknown constant source strengths can be determined from the following sets of algebraic equations

$$-2\pi\sigma_{1i} + \sum_{j=1}^{N}\sigma_{1j}\iint\limits_{\Delta S_j}\frac{\partial}{\partial n}\left[\frac{1}{R(\mathbf{r}_i,\,\mathbf{r}_j)}\right]\mathrm{d}S = \mathbf{u}(x_i, y_i, z_i)\cdot\mathbf{n}(x_i, y_i, z_i), \tag{24}$$

$$-2\pi\sigma_{2i} + \sum_{j=1}^{N}\sigma_{2j}\iint\limits_{\Delta S_j}\frac{\partial}{\partial n}\left[\frac{1}{R(\mathbf{r}_i,\,\mathbf{r}_j)}\right]\mathrm{d}S = \frac{\partial\mathbf{u}(x_i, y_i, z_i)}{\partial x}\cdot\mathbf{n}(x_i, y_i, z_i), \tag{25}$$

where ΔS_j represents the area of the jth panel, N is the number of panels required to discretize the wetted and image surfaces. σ_1 and σ_2 denotes the unknown constant source strengths of the potential functions ϕ_1 and ϕ_2, respectively.

It should be noted that the displacement vectors $\mathbf{u}(x_i, y_i, z_i)$ and their derivatives $\partial\mathbf{u}(x_i, y_i, z_i)/\partial x$ were obtained from the in vacuo finite element analysis.

2.4. Calculation of generalized fluid–structure interaction forces

Using the Bernoulli's equation and neglecting the second-order terms, the dynamic fluid pressure on the elastic structure due to the rth modal vibration becomes

$$P_r(x, y, z, t) = -\rho\left(\frac{\partial\phi_r}{\partial t} + U\frac{\partial\phi_r}{\partial x}\right). \tag{26}$$

Substituting Eq. (15) into Eq. (26), the following expression for the pressure is obtained:

$$P_r(x, y, z, t) = -\rho\left(\lambda\phi_r + U\frac{\partial\phi_r}{\partial x}\right)p_{0r}e^{\lambda t}. \tag{27}$$

By using the definition $\phi_r = \lambda\phi_{r1} + U\phi_{r2}$, Eq. (27) may be rewritten in the following form:

$$P_r(x, y, z, t) = -\rho\left(\lambda^2\phi_{r1} + U\lambda\left(\frac{\partial\phi_{r1}}{\partial x} + \phi_{r2}\right) + U^2\frac{\partial\phi_{r2}}{\partial x}\right)p_{0r}e^{\lambda t}. \tag{28}$$

The kth component of the generalized fluid–structure interaction force due to the rth modal vibration of the elastic structure subjected to axial flow can be expressed in terms of the pressure acting on the wetted surface of the structure as

$$\begin{aligned} Z_{kr}(t) &= \iint_{S_W} P_r(x, y, z, t)\mathbf{u}_k \cdot \mathbf{n}\,\mathrm{d}S \\ &= -p_{0r}e^{\lambda t}\iint_{S_W}\rho\left(\lambda^2\phi_{r1} + U\lambda\left(\frac{\partial\phi_{r1}}{\partial x} + \phi_{r2}\right) + U^2\frac{\partial\phi_{r2}}{\partial x}\right)\mathbf{u}_k \cdot \mathbf{n}\,\mathrm{d}S \\ &= -\lambda^2 p_{0r}e^{\lambda t}\rho\iint_{S_W}\phi_{r1}\mathbf{u}_k \cdot \mathbf{n}\,\mathrm{d}S - \lambda p_{0r}e^{\lambda t}\rho U\iint_{S_W}\left(\frac{\partial\phi_{r1}}{\partial x} + \phi_{r2}\right)\mathbf{u}_k \cdot \mathbf{n}\,\mathrm{d}S \\ &\quad - p_{0r}e^{\lambda t}\rho U^2\iint_{S_W}\frac{\partial\phi_{r2}}{\partial x}\mathbf{u}_k \cdot \mathbf{n}\,\mathrm{d}S. \end{aligned} \tag{29}$$

The generalized added mass A_{kr}, generalized fluid damping (due to the Coriolis effect of fluid), B_{kr}, and generalized fluid stiffness (due to the centrifugal effect of fluid), C_{kr}, coefficients can be defined as

$$A_{kr} = \rho\iint_{S_W}\phi_{r1}\mathbf{u}_k \cdot \mathbf{n}\,\mathrm{d}S, \tag{30}$$

$$B_{kr} = \rho U\iint_{S_W}\left(\frac{\partial\phi_{r1}}{\partial x} + \phi_{r2}\right)\mathbf{u}_k \cdot \mathbf{n}\,\mathrm{d}S, \tag{31}$$

$$C_{kr} = \rho U^2\iint_{S_W}\frac{\partial\phi_{r2}}{\partial x}\mathbf{u}_k \cdot \mathbf{n}\,\mathrm{d}S. \tag{32}$$

Therefore, the generalized fluid–structure interaction force component, Z_{kr}, can be rewritten as

$$\begin{aligned} Z_{kr}(t) &= -A_{kr}\lambda^2 p_{0r}e^{\lambda t} - B_{kr}\lambda p_{0r}e^{\lambda t} - C_{kr}p_{0r}e^{\lambda t} \\ &= -A_{kr}\ddot{p}_r(t) - B_{kr}\dot{p}_r(t) - C_{kr}p_r(t). \end{aligned} \tag{33}$$

2.5. Calculation of eigenvalues and eigenvectors

The generalized equation of motion for the elastic structure, in contact with axial flow and assuming vibrations with no structural damping, is

$$\left[\lambda^2(\mathbf{a}+\mathbf{A})+\lambda(\mathbf{B})+(\mathbf{c}+\mathbf{C})\right]\mathbf{p}=0, \tag{34}$$

where **a** and **c** denote the generalized structural mass and stiffness matrices, respectively. The matrices **A**, **B** and **C** represent the generalized added mass, generalized fluid damping and generalized fluid stiffness matrices, respectively.

It should be noticed that the eigenvalue λ is generally complex. It was observed from the solution of the eigenvalue problem that, before the onset of the instability, the eigenvalues have zero real part, and therefore, the fluid–structure interaction system is conservative. On the other hand, the eigenvectors **p** have both real and imaginary parts, which are different from zero. Therefore, the eigenvectors (modes) are complex. However, when the axial mean flow velocity is zero, the fluid–structure interaction forces are only due to the inertia of the fluid. These interaction effects are represented by a symmetric generalized added mass matrix, and, hence, the eigenvectors only have real parts.

3. Numerical results and comparisons

A series of calculations have been performed to demonstrate the applicability of the aforementioned theory to structures containing and/or submerged in flowing fluid. The structure adopted is a finite length circular cylindrical shell, and it is simply supported at both ends. The shell under consideration was analytically investigated by Weaver and Unny [25], Selmane and Lakis [26], Amabili et al. [9] and Amabili and Garziera [5]. The circular cylindrical shell adopted in the calculations has the geometric and material properties: length-to-radius ratio $L/R=2$, thickness-to-radius ratio $h/R=0.01$, Young's modulus $E=206\,\text{GPa}$, Poisson's ratio $v=0.3$, and mass density $\rho_s=7850\,\text{kg/m}^3$. Fresh water is used as the contained and/or surrounding fluid with a density of $\rho_f=1000\,\text{kg/m}^3$.

A right-handed Cartesian coordinate system, xyz, is adopted in the present study, and it is shown in Fig. 1 for the cylindrical shell subjected to axial flow. The coordinate system is fixed in space with its origin at O. The x-axis lies along the length L, and coincides with the centerline of the cylindrical shell.

For convenience, the following non-dimensional parameters are introduced as in Amabili and Garziera [5] and Weaver and Unny [25]:

$$V=U/\left\{(\pi^2/L)[D/(\rho h)]^{1/2}\right\},\quad \Omega=\lambda/\left\{(\pi^2/L^2)[D/(\rho h)]^{1/2}\right\}. \tag{35}$$

Here, V and Ω denote the non-dimensional axial fluid velocity and non-dimensional eigenfrequency, respectively, and λ is the corresponding complex eigenvalues of the cylindrical shell conveying and/or submerged in flowing fluid. Furthermore, D is the flexural rigidity, and it is defined as $D=Eh^3/12(1-v^2)$.

3.1. Convergence tests for finite element and boundary element mesh size

The in vacuo dynamic characteristics of the thin shell structure were obtained using the ANSYS finite element software [19]. This produces information on natural frequencies and normal mode shapes of the *dry* shell structure in vacuum. In these calculations, the cylindrical shell was discretized with four-noded quadrilateral shell elements, including both membrane and bending stiffness influences.

In a preliminary calculation, 512 elements were distributed over the shell structure. The distribution over the simply supported shell consists of 32 equally spaced elements around the circumference and 16 equally spaced elements along the length of the cylindrical shell. To test the convergence of the calculated dynamic properties, i.e., natural frequencies and normal mode shapes, the number of elements over the cylindrical shell surface was increased first to 1152 – 48 elements around the circumference and 24 elements along the shell and then to 2048 and 3200 elements, respectively. For the idealizations with 2048 and 3200 elements, respectively, 64 and 80 quadratic elements were distributed around the circumference, and 32 and 40 elements along the cylindrical shell. In a final test of idealization, the number of elements was increased to 96 and 50, respectively, around the circumference and along the cylindrical shell. Therefore, a total number of 4800 elements were distributed over the shell structure in this final idealization. Table 1 shows the predicted natural frequencies obtained from ANSYS, for 15 mode shapes. The mode shapes of the shell structure in vacuum are identified with the number of standing waves around the circumference, n, and the number of half-waves along the shell, m. A combination of m and n forms a particular mode shape (m, n). The results occur in pairs. That is, in general, for each natural frequency, there exists a pair of mode shapes satisfying the relevant orthogonality conditions. Therefore, in Table 1, one result is presented for each pair of mode shapes. The in

Table 1
Convergence of FEM natural frequencies (in vacuo) for cylindrical shell simply supported at its ends (Hz)

Mode (m, n)	512 elements idealization	1152 elements idealization	2048 elements idealization	3200 elements idealization	4800 elements idealization
1,5	96.4	96.1	96.0	96.0	96.0
2,5	244.1	242.0	241.2	240.9	240.7
3,5	403.7	398.6	396.5	395.6	395.1
4,5	530.1	524.2	521.4	520.2	519.6
5,5	620.9	618.1	616.1	615.2	615.0
1,6	105.2	104.8	104.7	104.6	104.6
2,6	207.1	205.3	204.8	204.5	204.4
3,6	346.7	341.4	339.4	338.6	338.1
4,6	475.8	467.4	464.0	462.5	461.8
5,6	580.6	572.0	568.1	566.6	565.8
1,7	130.3	129.5	129.3	129.2	129.1
2,7	197.3	195.9	195.5	195.4	195.3
3,7	312.3	307.5	306.0	305.3	305.0
4,7	435.5	426.3	423.0	421.6	420.9
5,7	547.0	535.1	530.5	528.5	527.7

Table 2
Convergence of wet natural frequencies for cylindrical shell completely filled with water (Hz)

Mode (m,n)	512 panels idealization	1152 panels idealization	2048 panels idealization	3200 panels idealization	4800 panels idealization
1,5	58.3	55.2	54.0	53.5	53.2
2,5	153.6	143.7	140.1	138.6	137.7
3,5	267.7	247.5	240.4	237.2	235.3
4,5	372.5	341.7	331.0	326.1	323.3
5,5	461.8	423.0	409.4	403.0	399.4
1,6	69.3	64.4	62.7	61.9	61.4
2,6	140.4	129.5	125.7	123.9	122.9
3,6	244.7	223.0	215.4	211.9	209.9
4,6	351.9	317.5	305.6	300.0	296.9
5,6	450.3	404.6	388.6	381.3	377.0
1,7	92.6	84.6	81.8	80.5	79.7
2,7	143.2	130.5	126.0	123.9	122.7
3,7	233.8	210.5	202.4	198.6	196.5
4,7	338.4	301.3	288.4	282.4	279.0
5,7	441.9	391.2	373.4	365.0	360.4

vacuo dynamic characteristics of the shell structure are scaled to a generalized mass of $1\,\mathrm{kg\,m^2}$. The differences in the results, shown in Table 1, indicate that the calculated values are slowly converging with increasing number of elements. The results of the final idealization (4800 elements) were adopted for the in vacuo dynamic characteristics of the cylindrical shell simply supported at both ends.

To test the convergence of the hydrodynamic predictions, various numbers of hydrodynamic panels were distributed around the circumference and along the length of the wetted surface of the cylindrical shell. The main aim of this exercise was to represent accurately the distortional mode shapes of the wetted surface area of the structure. For the cylindrical shell completely filled with a quiescent fluid (fresh water), five different idealizations of panel distribution over the wetted surface of the cylindrical structure were considered (see Table 2). The hydrodynamic panels were distributed over the wetted surface of the shell as follows: one structural element (finite element) corresponding to one hydrodynamic panel. Therefore, the same number of hydrodynamic panels and structural elements were adopted for the *wet* results presented for the completely filled shell (see Tables 1 and 2). Table 2 shows the convergence of the predicted *wet* frequencies with increasing number of hydrodynamic panels for 15 different mode shapes. It can be observed from Table 2 that the *wet* frequencies are converging slowly with increasing number of hydrodynamic panels. The differences between the last two idealizations (3200 and 4800 hydrodynamic panel idealizations) are reasonably small for all the mode shapes presented. Therefore, it may be said that the final idealization (4800 hydrodynamic panel idealization) adequately represents the distortional mode shapes of the circular cylindrical shell completely filled with a quiescent fluid (fresh water).

For the shell structure filled with flowing water, another convergence study was performed in order to establish the number of panels necessary to obtain the converged fluid–structure interaction effects, e.g., generalized added mass coefficients, generalized Coriolis force coefficients

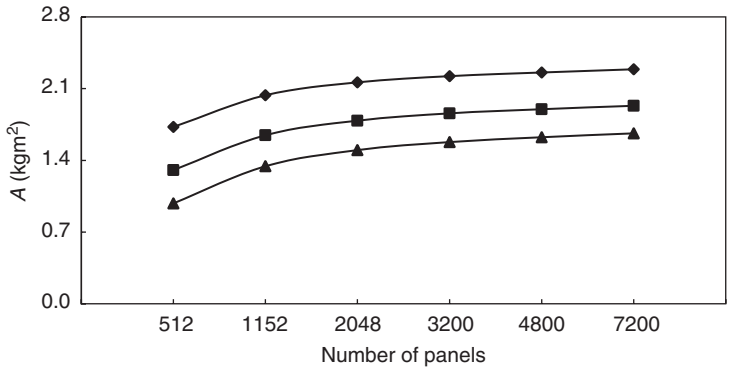

Fig. 3. Convergence of generalized added mass values. *Key*: —◆—, ($m = 1$, $n = 5$); —■—, ($m = 1$, $n = 6$); —▲—, ($m = 1$, $n = 7$).

and generalized centrifugal force coefficients. Fig. 3 presents the diagonal terms of the generalized added mass matrix for the mode shapes ($m = 1$, $n = 5$), ($m = 1$, $n = 6$) and ($m = 1$, $n = 7$), for six different hydrodynamic panel idealizations. It should be noted that the generalized added mass coefficients associated with the distortional in vacuo modes are a function of the number of waves around the circumference and the number of half-waves along the cylindrical shell (see, for instance, [21]). The generalized added mass values presented in Fig. 3 are obtained for the in vacuo modes scaled to a generalized structural mass of 1 kg m^2. It can also be seen from Fig. 3 that the generalized added mass terms converge with increasing number of hydrodynamic panels. The results of the 4800 hydrodynamic panels idealization may be assumed reasonably converged, and they were adopted throughout the calculations.

Furthermore, Figs. 4 and 5 show, respectively, the generalized Coriolis force and generalized centrifugal force coefficients for the non-dimensional axial flow velocities $V = 1$, 2 and 3, and for six different hydrodynamic panel idealizations. The generalized Coriolis force coefficients matrix is skew symmetric, and the coefficients presented in Figs. 4(a)–(c) represent the coupling between the modes ($m = 1$, $n = 5$) and ($m = 2$, $n = 5$), ($m = 1$, $n = 6$) and ($m = 2$, $n = 6$), and ($m = 1$, $n = 7$) and ($m = 2$, $n = 7$), respectively. On the other hand, Figs. 5(a)–(c) present the generalized centrifugal fluid force coefficients for the diagonal terms ($m = 1$, $n = 5$), ($m = 1$, $n = 6$) and ($m = 1$, $n = 7$), respectively. All the generalized fluid force coefficients presented in Figs. 4 and 5 are normalized according to a generalized structural mass of 1 kg m^2. It may also be observed from Figs. 4 and 5 that the generalized fluid–structure interaction force coefficients are converging slowly with increasing number of hydrodynamic panels for the non-dimensional fluid velocities $V = 1$, 2 and 3. The fluid–structure interaction force coefficients (Coriolis and centrifugal) may be assumed sufficiently converged for the 4800 hydrodynamic panels idealization, and therefore, they were adopted for the dynamic properties of the cylindrical shell completely filled with and/or submerged in flowing fluid.

3.2. Calculated results and comparisons

By solving the eigenvalue problem, Eq. (34), the non-dimensional eigenvalues and associated eigenmodes of the cylindrical shell containing and/or submerged in flowing fluid are obtained as a

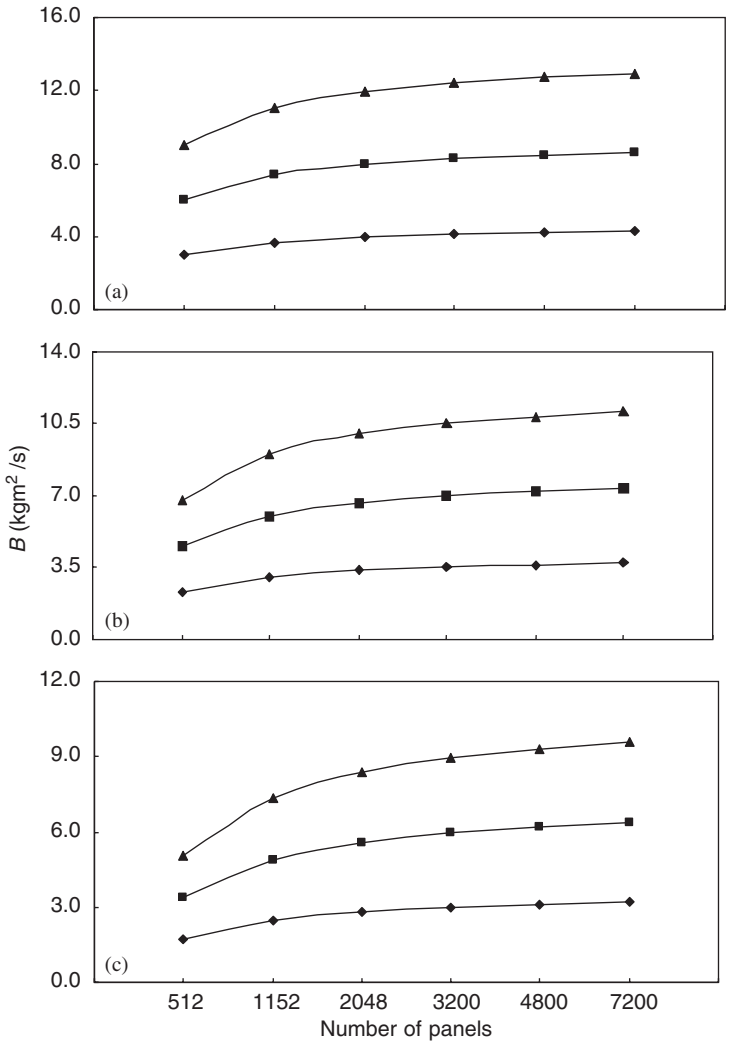

Fig. 4. Convergence of generalized Coriolis force coefficients (off-diagonal terms) due to coupling between in vacuo modes: (a) ($m = 1$, $n = 5$) and ($m = 2$, $n = 5$); (b) ($m = 1$, $n = 6$) and ($m = 2$, $n = 6$); (c) ($m = 1$, $n = 7$) and ($m = 2$, $n = 7$). Key: —◆—, $V = 1$; —■—, $V = 2$; —▲—, $V = 3$.

function of the non-dimensional flow velocity. The predictions based on the proposed method are compared with the analytical calculations reported by Weaver and Unny [25], Selmane and Lakis [26], Amabili et al. [9] and Amabili and Garziera [5]. For the cylindrical shell subjected to flowing water, the predictions of the proposed method are presented for various numbers of *wet* modes. For the results presented in Figs. 6–14, a maximum number of 134 in vacuo modes were included in the analysis—67 of which were symmetric and 67 antisymmetric with respect to the symmetry plane through the center of the shell and perpendicular to the free surface of the fluid (see Figs. 1 and 2). However, 80 in vacuo normal modes—40 of which symmetric and 40 antisymmetric were adopted for the calculations concerning the cylindrical shell completely filled with flowing fluid.

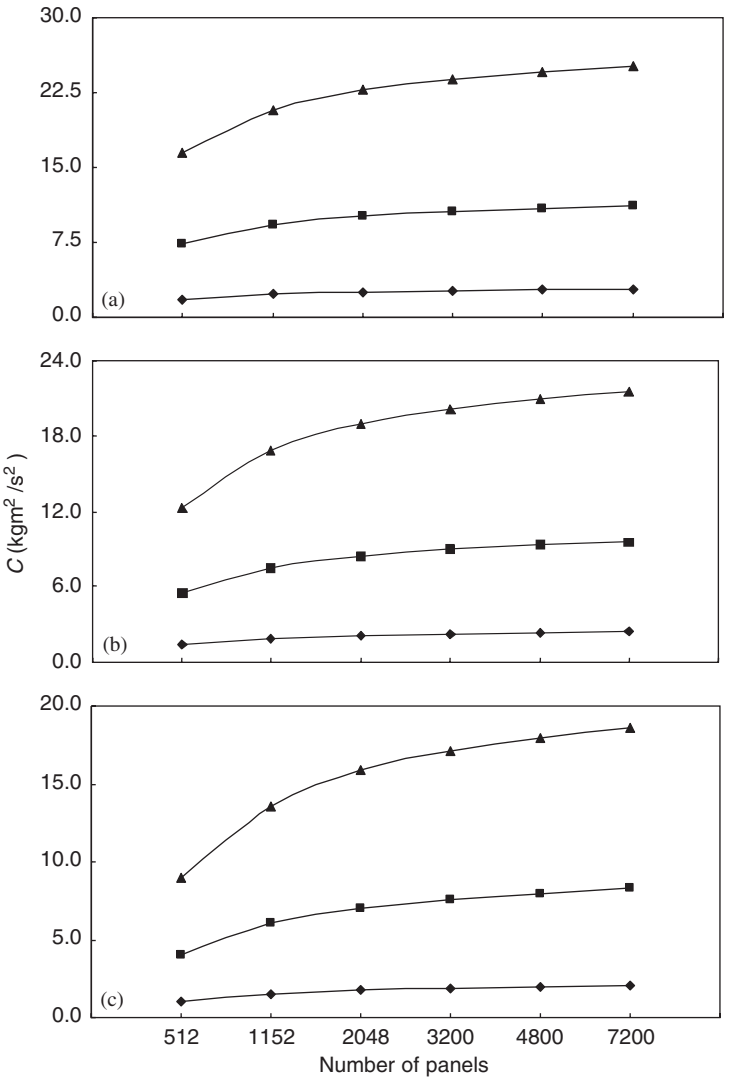

Fig. 5. Convergence of generalized centrifugal force coefficients (diagonal terms): (a) mode ($m = 1$, $n = 5$); (b) mode ($m = 1$, $n = 6$); (c) mode ($m = 1$, $n = 7$). Key: —◆—, $V = 1$; —■—, $V = 2$; —▲—, $V = 3$.

Figs. 6(a) and (b) compare the imaginary parts of the predicted non-dimensional eigenvalues with those obtained by Weaver and Unny [25] and Amabili et al. [9], respectively, for the first two modes having five circumferential waves ($n = 5$). The results presented in Figs. 6(a) and (b) correspond to the cylindrical shell with rigid extensions. This is to say that the flexible cylindrical shell is connected to infinitely long rigid cylindrical baffles, of the same diameter as the shell, at both ends. For the results of the present study in Figs. 6(a) and (b), two groups of calculations were performed. In the first group of calculations, only the flexible cylindrical shell, simply supported at both ends, was modeled, and it was discretized by 4800 hydrodynamic panels. No

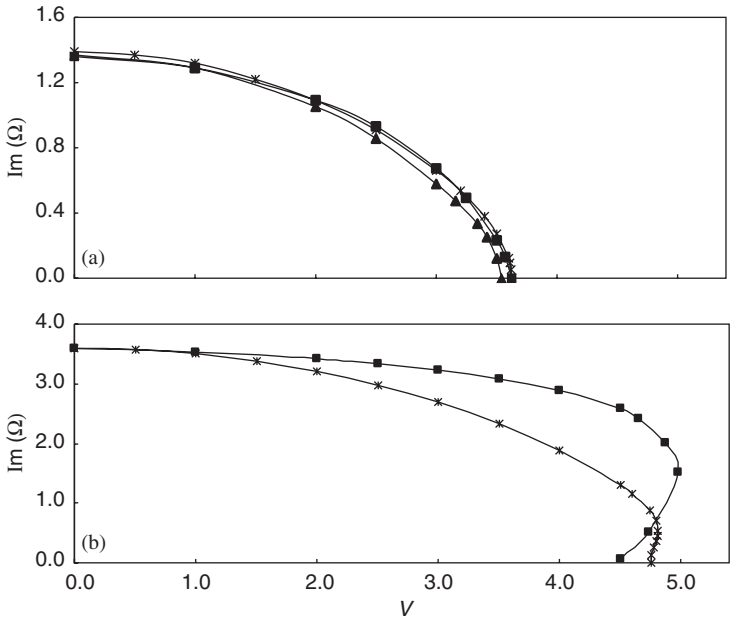

Fig. 6. Imaginary parts of non-dimensional eigenfrequencies for flowing fluid conveying cylindrical shell with rigid extensions, for $n = 5$: (a) first mode; (b) second mode. *Key*: —▲—, Ref. [9]; —■—, Ref. [25]; —✳—, this study.

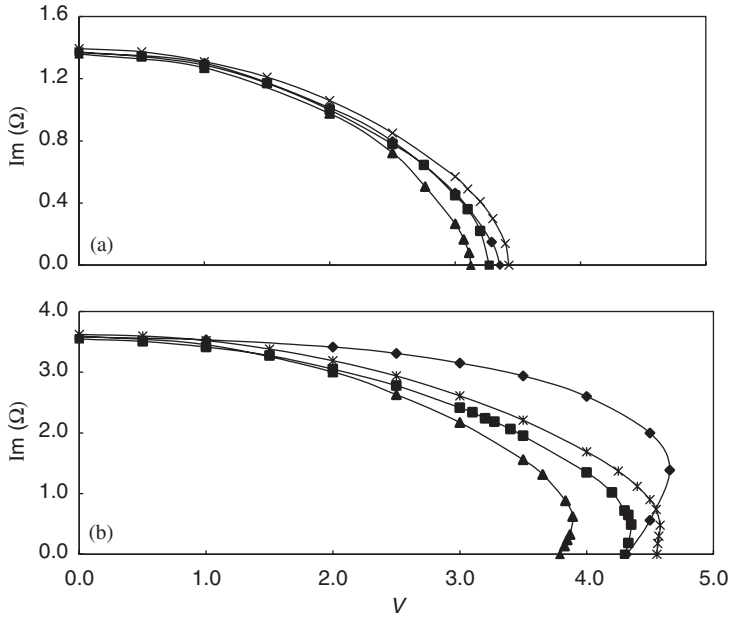

Fig. 7. Imaginary parts of non-dimensional eigenfrequencies for flowing fluid conveying cylindrical shell with flexible extensions, for $n = 5$: (a) first mode; (b) second mode. *Key*: —▲—, Ref. [26]; —◆—, Ref. [9]; —■—, Ref. [5]; —✳—, this study.

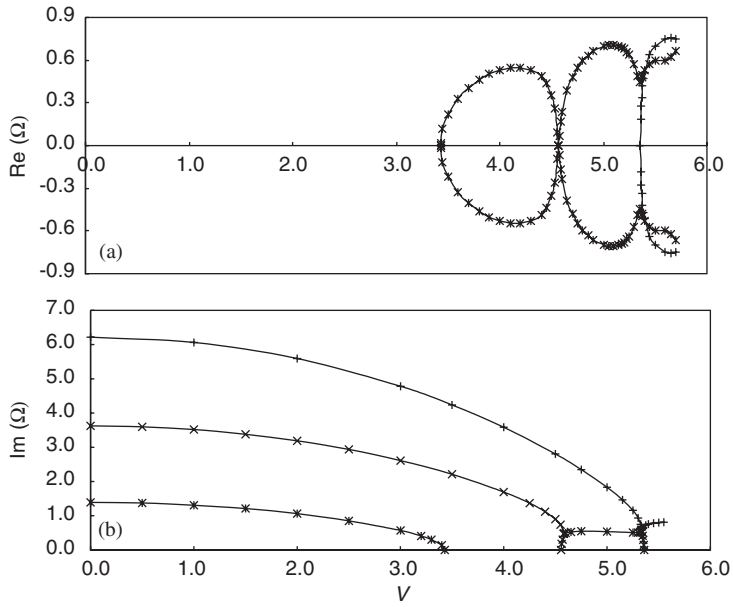

Fig. 8. Non-dimensional eigenvalues of cylindrical shell conveying flowing fluid, for $n = 5$: (a) real parts; (b) imaginary parts. *Key*: —✳—, first mode; —×—, second mode; —|—, third mode.

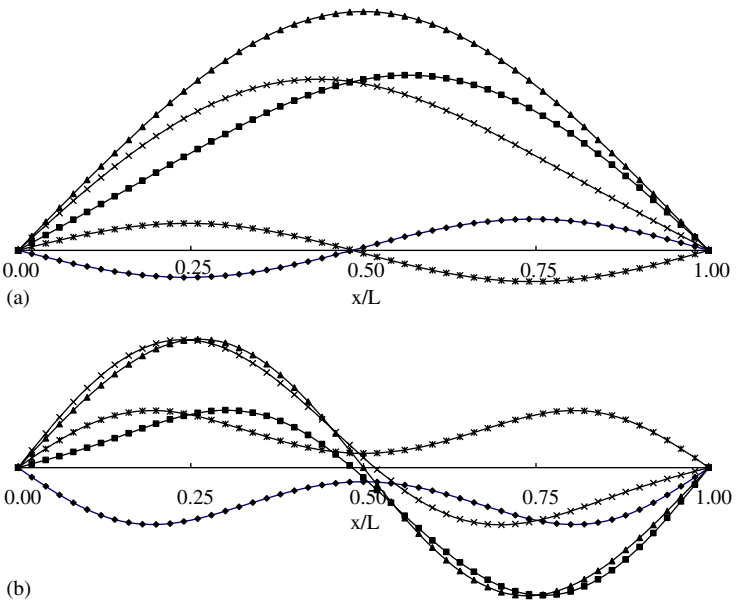

Fig. 9. Eigenmodes of cylindrical shell conveying flowing fluid, for $n = 5$ and $V = 1.72$: (a) first mode; (b) second mode. *Key*: —◆—, $t = 0$; —■—, $t = T/8$; —▲—, $t = T/4$; —×—, $t = 3T/8$; —✳—, $t = T/2$ (T is period).

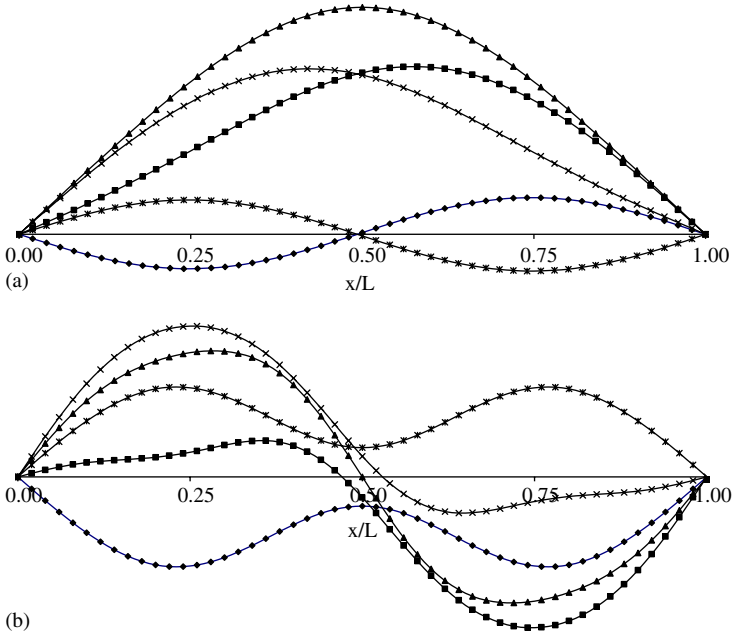

Fig. 10. Eigenmodes of cylindrical shell conveying flowing fluid, for $n = 5$ and $V = 2.57$: (a) first mode; (b) second mode. *Key*: —◆—, $t = 0$; —■—, $t = T/8$; —▲—, $t = T/4$; —×—, $t = 3T/8$; —✳—, $t = T/2$ (T is period).

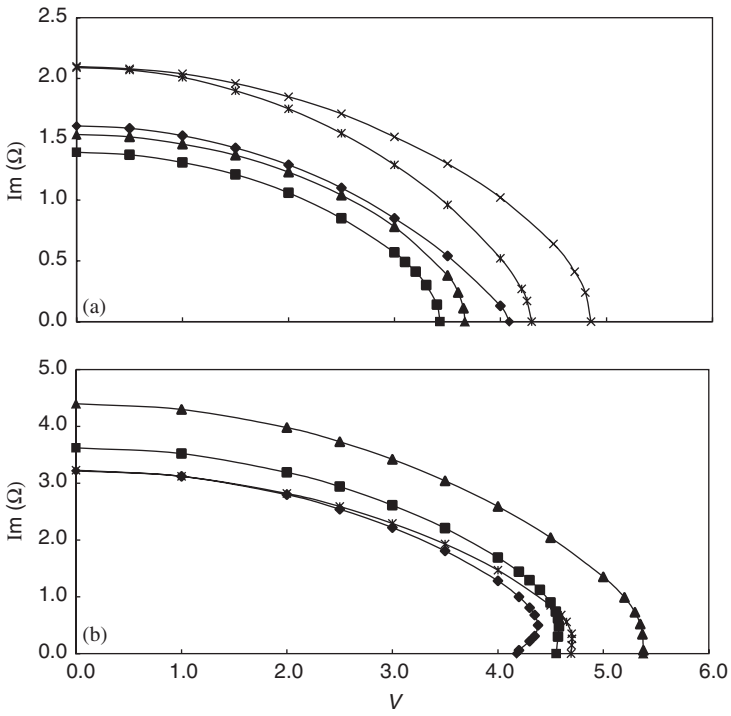

Fig. 11. Imaginary parts of non-dimensional eigenfrequencies for cylindrical shell conveying flowing fluid: (a) first mode; (b) second mode. *Key*: —×—, $n = 3$; —▲—, $n = 4$; —■—, $n = 5$; —◆—, $n = 6$;—✳—, $n = 7$.

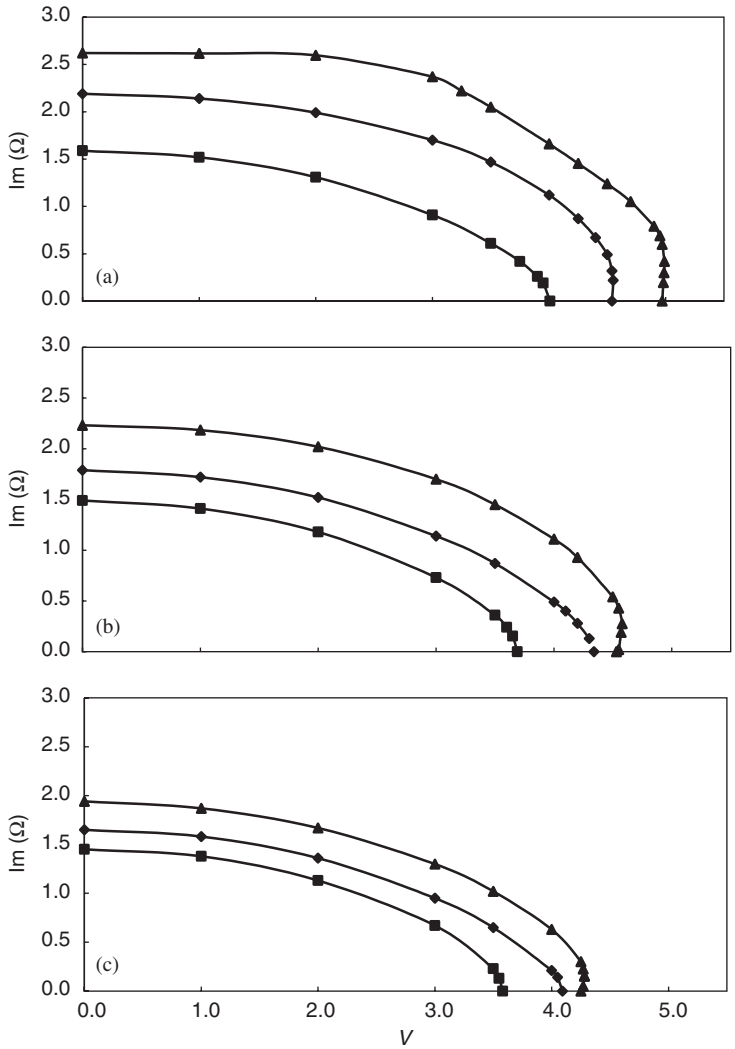

Fig. 12. Imaginary parts of non-dimensional eigenfrequencies for cylindrical shell partially filled with flowing fluid: (a) $\frac{1}{4}$-filled; (b) $\frac{1}{2}$-filled; (c) $\frac{3}{4}$-filled. *Key*: —■—, first mode; —◆—, second mode; —▲—, third mode.

boundary condition was imposed beyond the ends of the shell at $x = 0$ and L. This means that the effect of the rigid baffles beyond the simply supported ends was not taken into account in the calculation of the hydrodynamic forces. In the second group of calculations, the flexible shell was discretized together with the rigid cylindrical baffles, of the same length and diameter as the shell structure, at both ends. A number of 4800 hydrodynamic panels was adopted separately for the each rigid baffle, and the same number of panels was also distributed over the shell structure. Therefore, a total number of 14 400 hydrodynamic panels was adopted for the shell-rigid baffles system. The kinematic boundary condition (Eqs. (22) and (23)) was imposed on the flexible shell,

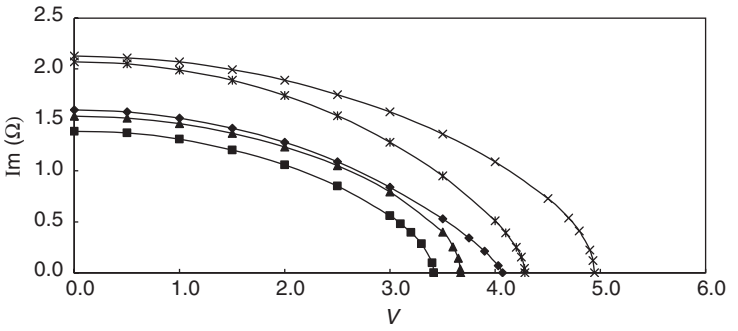

Fig. 13. Imaginary parts of nondimensional eigenfrequencies for empty cylindrical shell submerged in flowing fluid. *Key*: —×—, $n = 3$; —▲—, $n = 4$; —■—, $n = 5$; —◆—, $n = 6$; —✳—, $n = 7$.

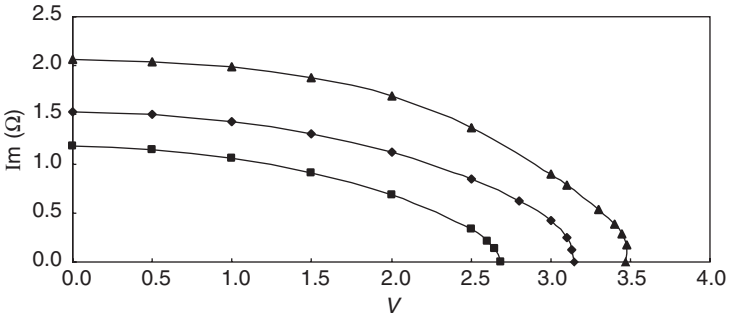

Fig. 14. Imaginary parts of nondimensional eigenfrequencies for cylindrical shell half-filled and $\frac{1}{4}$-submerged in flowing fluid. *Key*: —■—, first mode; —◆—, second mode; —▲—, third mode.

and the rigid boundary wetted surface condition $\partial\phi/\partial\mathbf{n} = 0$ was employed for the rigid extensions. It was observed from the analysis that two groups of calculations give almost the same results. Therefore, only one group of the calculations is presented in Figs. 6(a) and (b). It may also be observed from Figs. 6(a) and (b) that the non-dimensional eigenfrequencies decrease with increasing non-dimensional fluid velocity, and the first axial mode reaches zero frequency at the non-dimensional fluid velocity, V, 3.62 (see Fig. 6(a)). This point ($V = 3.62$) corresponds to the static divergence of the cylindrical shell filled with flowing water. The intersection of the second mode with the non-dimensional velocity axis ($V = 4.82$) gives the point of restabilization for the shell–fluid system. It may be seen from Figs. 6(a) and (b) that the results of the present study compare reasonably well with the analytical predictions of Weaver and Unny [25] and Amabili et al. [9]. However, the differences increase between the predictions of this study and those of Weaver and Unny [25], especially for the second mode, as the flow velocity increases. This may be due to the use of too few terms in the calculations by Weaver and Unny [25]. For the results presented (Figs. 6(a) and (b)), seven in vacuo modes with the axial half-wavenumbers $m = 1-7$ were taken into account. However, only, the first three and four longitudinal in vacuo modes become influential for the *wet* modes presented in Figs. 6(a) and (b), respectively.

In a further study, the effect of the flexible extensions was taken into account in the calculations of the generalized hydrodynamic properties, e.g., the generalized added mass coefficients, generalized Coriolis force coefficients and generalized centrifugal force coefficients. The cylindrical shell structure was assumed infinitely long and periodically supported, and a three-span length of the infinitely long flexible structure was adopted for the calculations. It was assumed that mode shapes are periodic functions with main period $2L$. Therefore, the mode shapes were antisymmetric with respect to each support, and they were the mode shapes with the lowest frequencies (see, for instance, Ref. [5]). The each span of the adopted structure was discretized by using 4800 hydrodynamic panels, and a total number of 14 400 hydrodynamic panels was distributed over the three-span cylindrical structure for the calculations. The hydrodynamic force calculations were performed for the mid-span section of the three-span cylindrical shell structure. The effect of the structural vibrations in the fore and aft spans, on the shell structure in the mid-span, was calculated in terms of the hydrodynamic force coefficients, i.e., the generalized added mass coefficients, Coriolis fluid force coefficients and centrifugal fluid force coefficients. The imaginary parts of the predicted non-dimensional eigenvalues are presented in Figs. 7(a) and (b), respectively, for the first two axial modes with $n = 5$. In these figures (Figs. 7(a) and (b)), the predicted frequency values are compared with the analytical calculations of Amabili and Garziera [5], Amabili et al. [9] and Selmane and Lakis [26]. It can be observed from Figs. 7(a) and (b) that the predictions compare reasonably well with those of Amabili and Garziera [5], Amabili et al. [9] and Selmane and Lakis [26]. As noted before, the imaginary part of the non-dimensional eigenfrequency decreases with increasing non-dimensional flow velocity, and the first axial mode (see Fig. 7(a)) reaches zero frequency at the non-dimensional flow velocity, V, 3.43. However, there are some differences between the predictions of this study and those found in the literature, especially for the second mode, as the critical flow velocity approached. This indicates that the non-dimensional frequency values become more sensitive to the formulation of the problem as the flow velocity increases.

Figs. 8(a) and (b) present, respectively, the real and imaginary parts of the non-dimensional eigenfrequency, as a function of the non-dimensional flow velocity, for the first three axial modes with the circumferential wavenumber, n, 5. For the results giving in these figures, the cylindrical shell is considered with flexible extensions. In other words, three successive spans of the periodically supported infinite long shell structure were adopted for the calculations. As seen in Fig. 8(b), the imaginary part of the non-dimensional eigenfrequency decreases with increasing non-dimensional axial flow velocity. The lowest mode shape reaches its zero frequency at $V = 3.43$, and the intersection of the second mode with the axis of non-dimensional flow velocity at $V = 4.55$ is the point of restabilization. Then, the first and second modes merge at $V = 4.58$, and this point corresponds to the onset of the coupled-mode flutter. It should also be noted that the coupled-mode flutter cannot be decided by the linear theory (see, for instance, Refs. [5,9]). Furthermore, the real part of the non-dimensional eigenfrequency is presented in Fig. 8(a) as a function of the non-dimensional flow velocity, and it is proportional to damping. It should also be noted that the system is stable when the real part of the non-dimensional frequency (Ω) is negative, and it is unstable when the real part of Ω is positive.

Figs. 9 and 10 present the mode shapes of the cylindrical shell completely filled with flowing fluid at the times $t = 0$, $T/8$, $T/4$, $3T/8$ and $T/2$ (where T is the time period) for the non-dimensional flow velocities $V = 1.72$ and 2.57, respectively. The first and second axial mode

shapes with the circumferential wavenumber, n, 5 are shown, respectively, in Figs. 9(a) and (b) for $V = 1.72$, and in Figs. 10(a) and (b) for $V = 2.57$. It should also be noted that the mode shapes are complex. The real part of the first eigenvector has one longitudinal half-wave and the imaginary part has two longitudinal half-waves (see, mode shapes at $t = 0$ and $T/2$ in Figs. 9(a) and 10(a)). On the other hand, the imaginary part of the second mode shape involves the longitudinal mode with $m = 3$ (see mode shapes at $t = 0$ and $T/2$ in Figs. 9(b) and 10(b)). From the comparison of Figs. 9 and 10, it can be said that the mode shapes demonstrate similar characteristics for the non-dimensional axial flow velocities $V = 1.72$ and 2.57.

Furthermore, the eigenvalues of the shell structure completely filled with flowing fluid were calculated for different circumferential wavenumbers. For the circumferential wavenumbers, n, 3–7, Figs. 11(a) and (b) present the imaginary parts of the non-dimensional eigenfrequencies for the first two axial modes, respectively. The non-dimensional eigenfrequency values decrease with increasing non-dimensional fluid velocity, as seen in Figs. 11(a) and (b). The first modes reach zero values at $V = 4.86$, 3.66, 3.43, 4.08 and 4.30, respectively, for the circumferential wavenumbers, n, 3, 4, 5, 6 and 7 (see Fig. 11(a)). These non-dimensional flow velocities corresponding to zero eigenfrequenies are the critical flow velocities for static divergence of the modes. These modes gain their stabilities at $V = 5.38$, 4.55, 4.18 and 4.69 for $n = 4$, 5, 6 and 7, respectively (see Fig. 11(b)). It may also be observed from Figs. 11(a) and (b) that the highest frequencies are observed for the circumferential wavenumber, n, 3, and the lowest ones for $n = 5$ and 6, respectively, for the first and second modes.

In a separate analysis, the effect of the flowing fluid partially in contact with the cylindrical shell structure was investigated. Figs. 12(a)–(c) present the imaginary parts of the non-dimensional eigenfrequencies, respectively, for the $\frac{1}{4}$-filled, $\frac{1}{2}$-filled and $\frac{3}{4}$-filled cylindrical shells. The results are presented for the first three axial mode shapes. The non-dimensional frequencies behave as expected from the theory. That is to say that the imaginary parts of the non-dimensional frequencies decrease with increasing area of contact with the fluid. The largest area of contact was in the case of the $\frac{3}{4}$-filled shell, and therefore, the lowest frequencies were observed for this case. For the partially filled structure, the image method was employed in order to satisfy the appropriate boundary condition on the free surface ($\phi = 0$). For the cases of the $\frac{1}{4}$-filled, $\frac{1}{2}$-filled and $\frac{3}{4}$-filled shells, 9600, 14 400 and 19 200 hydrodynamic panels, respectively, were adopted for the calculations. A maximum number of 134 in vacuo normal modes – 67 of which were symmetric and 67 antisymmetric with respect to the plane passing through the center of the shell and perpendicular to the free surface was included in the analysis.

In a further study, the effect of the external flow on the dynamic behavior of the shell structure with flexible extensions was investigated. The imaginary parts of the non-dimensional eigenfrequencies are presented in Fig. 13 for the empty shell structure completely submerged in flowing water. The results are presented for the first axial modes with the circumferential wavenumbers, n, 3–7. The lowest frequencies, again, were obtained for the circumferential wavenumber, n, 5, and the highest values for $n = 3$. For the completely submerged and empty cylindrical shell, the divergence occurs at the non-dimensional axial flow velocities, $V = 4.94$, 3.67, 3.42, 4.07 and 4.28, respectively, for the circumferential wavenumbers, n, 3, 4, 5, 6 and 7.

On the other hand, in a separate analysis, the cylindrical shell was assumed partially filled with and partially submerged in flowing fluid. Fig. 14 presents the imaginary parts of the non-dimensional frequency values for the half-filled and $\frac{1}{4}$-submerged cylindrical shell. The results in

Fig. 14 are presented for the first three mode shapes. The imaginary parts of the non-dimensional eigenfrequencies presented in Fig. 14 are lower than those corresponding to the $\frac{3}{4}$-filled cylindrical shell (see Fig. 12(c)).

4. Conclusions

A method of analysis is presented for the response behavior of elastic structures partially filled with and/or partially submerged in flowing fluid. The method of analysis is based on a boundary integral equation method and the method of images. An elastic circular cylindrical shell structure, partially filled with and/or submerged in flowing water, was chosen in order to demonstrate the applicability of the method. It can be concluded from the results presented that the method proposed is suitable for the vibration analysis of flexible structures subjected to flowing fluid.

The in vacuo dynamic characteristics (i.e., natural frequencies and normal mode shapes) of the cylindrical structure were obtained by using the finite element idealization of 96 elements around the circumference and 50 elements along the shell structure. A maximum number of 134 in vacuo modes – 67 symmetric and 67 antisymmetric were calculated by using the ANSYS finite element software. They were included in the *wet* part of the analysis for the shell structure partially in contact with flowing fluid, and eighty in vacuo normal modes, only, were adopted for the calculations concerning the cylindrical shell completely filled with flowing fluid.

Throughout the calculations, the normal velocities on the wetted surface were expressed in terms of modal structural displacements, obtained from the in vacuo dynamic analysis. However, it should be noted that the normal fluid velocities cannot be arbitrarily specified. They have to satisfy the incompressibility condition (20). It must be realized that the method employed in this study cannot take into account the effect of compressibility.

The simply supported shell structure was considered with rigid and flexible extensions, and the predictions of the proposed method were compared with the analytical results found in the literature. The non-dimensional eigenfrequencies were presented as a function of the non-dimensional axial fluid velocity. The results were presented for various axial modes and circumferential wave numbers. The imaginary parts of the eigenfrequencies decrease with increasing fluid velocity, and they reach zero values at certain axial fluid velocities. The predicted points of static divergence compare reasonably well with those found in the literature.

For the cylindrical shell conveying flowing fluid, the mode shapes are complex. The first and second modes were presented at the times $t = 0$, $T/8$, $T/4$, $3T/8$ and $T/2$ (where T is the time period) for the shell completely filled with flowing water.

The calculations were also performed for the cylindrical shell partially filled and submerged in flowing water. The imaginary parts of the non-dimensional eigenvalues were presented for various filling ratios. The calculated frequency values behave as expected. That is to say that the frequencies decrease with increasing area of contact with flowing fluid.

The present study has demonstrated the versatility of the method developed through a cylindrical shell simply supported at both ends and subjected to flowing water. However, in order to obtain the converged hydrodynamic properties, a number of 4800 hydrodynamic panels were adopted in the calculations for the cylindrical shell completely filled with flowing fluid.

The structural and fluid idealizations are independent and both depending on the complexity of the structure and the convergence of the results. To test the convergence of the *wet* results, various numbers of hydrodynamic panels and in vacuo normal modes were adopted in the calculations. It is realized from the results presented that the non-dimensional *wet* frequencies converge slowly with increasing number of hydrodynamic panels. However, by using a higher-order source strength distribution (for instance, linearly varying source strength distribution) over the hydrodynamic panels, similar convergences can be achieved by using less number of panels. The results of the preliminary calculations using the higher order source strength distributions are encouraging, and they will be reported in future publications.

Acknowledgment

This research was financially supported by the Scientific and Technical Research Council of Turkey (TUBITAK Project No. 102I028). This support is gratefully acknowledged.

References

[1] M.P. Païdoussis, Flow-induced instabilities of cylindrical structures, *Applied Mechanics Reviews* 40 (1987) 163–175.
[2] M.P. Païdoussis, G.X. Li, Pipes conveying fluid: a model dynamical problem, *Journal of Fluids and Structures* 7 (1993) 137–204.
[3] M.P. Païdoussis, *Fluid–Structure Interactions: Slender Structures and Axial Flow*, Vol. I, Academic Press, London, 1998.
[4] M.P. Païdoussis, *Fluid–Structure Interactions: Slender Structures and Axial Flow*, Vol. II, Elsevier, The Netherlands, 2004.
[5] M. Amabili, R. Garziera, Vibrations of circular cylindrical shells with nonuniform constraints, elastic bed and added mass Part II: shells containing or immersed in axial flow, *Journal of Fluids and Structures* 16 (2002) 31–51.
[6] M.P. Païdoussis, E. Grinevich, D. Adamovic, C. Semler, Linear and nonlinear dynamics of cantilevered cylinders in axial flow, Part 1: physical dynamics, *Journal of Fluids and Structures* 16 (2002) 691–713.
[7] J.L. Lopes, M.P. Païdoussis, C. Semler, Linear and nonlinear dynamics of cantilevered cylinders in axial flow, Part 2: the equations of motion, *Journal of Fluids and Structures* 16 (2002) 715–737.
[8] C. Semler, J.L. Lopes, N. Augu, M.P. Païdoussis, Linear and nonlinear dynamics of cantilevered cylinders in axial flow, Part 3: nonlinear dynamics, *Journal of Fluids and Structures* 16 (2002) 739–759.
[9] M. Amabili, F. Pellicano, M.P. Païdoussis, Non-linear dynamics and stability of circular cylindrical shells containing flowing fluid, Part I: stability, *Journal of Sound and Vibration* 225 (1999) 655–699.
[10] M. Amabili, F. Pellicano, M.P. Païdoussis, Nonlinear stability of circular cylindrical shells in annular and unbounded axial flow, *Journal of Applied Mechanics American Society of Mechanical Engineers* 68 (2001) 827–834.
[11] M. Amabili, F. Pellicano, M.P. Païdoussis, Non-linear dynamics and stability of circular cylindrical shells conveying flowing fluid, *Computers and Structures* 80 (2002) 899–906.
[12] A.A. Lakis, A. Selmane, Hybrid finite element analysis of large amplitude vibration of orthotropic open and closed cylindrical shells subjected to a flowing fluid, *Nuclear Engineering and Design* 196 (2000) 1–15.
[13] M.H. Toorani, A.A. Lakis, Shear deformations in dynamic analysis of anisotropic laminated open cylindrical shells filled with or subjected to a flowing fluid, *Computer Methods in Applied Mechanics and Engineering* 190 (2001) 4929–4966.
[14] M.H. Toorani, A.A. Lakis, Dynamic analysis of anisotropic cylindrical shells containing flowing fluid, *Journal of Pressure Vessel Technology American Society of Mechanical Engineers* 123 (2001) 454–460.

[15] M.H. Toorani, A.A. Lakis, Dynamics behavior of axisymmetric and beam-like anisotropic cylindrical shells conveying fluid, *Journal of Sound and Vibration* 259 (2003) 265–298.
[16] A. Ergin, P. Temarel, Free vibration of a partially liquid-filled and submerged, horizontal cylindrical shell, *Journal of Sound and Vibration* 254 (2002) 951–965.
[17] A. Ergin, B. Uğurlu, Linear vibration analysis of cantilever plates partially submerged in fluid, *Journal of Fluids and Structures* 17 (2003) 927–939.
[18] A. Ergin, B. Uğurlu, Hydroelastic analysis of fluid storage tanks by using a boundary integral equation method, *Journal of Sound and Vibration* 275 (2004) 489–513.
[19] ANSYS, *User's Manual*, ANSYS, Inc., Houston, 1994.
[20] A. Ergin, The response behaviour of a submerged cylindrical shell using the doubly asymptotic approximation method (DAA), *Computers and Structures* 62 (1997) 1025–1034.
[21] A. Ergin, W.G. Price, R. Randall, P. Temarel, Dynamic characteristics of a submerged, flexible cylinder vibrating in finite water depths, *Journal of Ship Research* 36 (1992) 154–167.
[22] F. Kito, *Principles of Hydro-Elasticity*, Keio University Publications, Tokyo, 1970.
[23] J.L. Hess, A.M.O. Smith, Calculation of potential flow about arbitrary bodies, *Progress in Aeronautical Sciences*, Vol. 8, 1967, pp. 1–138.
[24] J.L. Hess, Review of integral-equation techniques for solving potential-flow problems with emphasis on the surface source method, *Computer Methods in Applied Mechanics and Engineering* 5 (1975) 145–196.
[25] D.S. Weaver, T.E. Unny, On the dynamic stability of fluid-conveying pipes, *Journal of Applied Mechanics American Society of Mechanical Engineers* 40 (1973) 48–52.
[26] A. Selmane, A.A. Lakis, Vibration analysis of anisotropic open cylindrical shells subjected to a flowing fluid, *Journal of Fluids and Structures* 11 (1997) 111–134.